Article

Bidirectional Acoustic Negative Refraction Based on a Pair of Identical Purely Imaginary Metamaterials Slabs

Ling-Ling Zhang [1,*], Yang Ji [2], Peng Chen [1], Qian Dai [1] and Xiao-Jun Liu [3,4,*]

[1] School of Network and Communication Engineering, Jingling Institute of Technology, Nanjing 211169, China
[2] College of Science, Hohai University, Nanjing 210093, China
[3] Key Laboratory of Modern Acoustics, Department of Physics and Collaborative Innovation Center of Advanced Microstructures, Nanjing University, Nanjing 210093, China
[4] State Key Laboratory of Acoustics, Institute of Acoustics, Chinese Academy of Sciences, Beijing 100190, China
* Correspondence: lindazhang@jit.edu.cn (L.-L.Z.); liuxiaojun@nju.edu.cn (X.-J.L.)

Abstract: Acoustic purely imaginary metamaterials (PIMs) slabs can support the coexistence of coherent perfect absorption and laser modes and are used to achieve negative refraction. Previous works have focused on a pair of different PIM slabs, one operating in CPA mode and the other in laser mode. However, this structure has restrictions on the incident wave direction, specifically the wave can only be incident from the CPA side. In this paper, we derive the analytical expressions for the parameters required for the coexistence of CPA and laser modes in acoustic PIM slabs. Numerical simulation results show that such PIM slab can freely switch states between the coherent complete absorber and the laser depending on the incidence direction. On this basis, by using a pair of identical PIM slabs, bidirectional negative refraction and planar focusing can be achieved. In addition, the parameters in the appropriate range can be found by adjusting the mode order, which facilitates the experimental verification. So far, the required acoustic purely imaginary metamaterials (PIMs) have not been experimentally demonstrated, and the results presented in the manuscript are theoretical speculations on their existence, so practical applications may require more sophisticated design and engineering.

Keywords: purely imaginary metamaterials (PIMs); acoustic laser; acoustic coherent perfect absorption (CPA); negative refraction; planar focusing

1. Introduction

A beam of light is refracted at the interface of any two homogeneous materials, and the refraction angle follows the Snell's law. In natural materials, both the refracted and incident light lie on either side of the normal. Metamaterials can be engineered to exhibit negative refraction, i.e., the refracted light is located on the same side of the normal as the incident light [1]. Negative refraction has attracted a lot of attention because it has exciting applications in various fields [2–6], such as antenna technology, electromagnetic absorbers, phase compensation, subwavelength lithography, and planar focusing lenses. The practical implementation of Negative refraction can be achieved using a slab possessing both negative permittivity and negative permeability [7–9]. However, negative refraction based on bulk double negative (DNG) metamaterials suffer from inherent challenges such as losses, limited granularity and non-ideal anisotropy, which hinder their applicability. Therefore, the idea of negative refraction has inspired a large number of studies aimed at introducing alternative approaches, such as using phase-conjugating interfaces [10,11], constructing phononic crystals [12–15], employing a pair of parity-time (PT) symmetric metasurfaces [5,16,17], etc. In particular, the coexistence of CPA and laser modes in PT symmetric systems can be achieved by adjusting the material parameters and structural configuration. In this active scheme, the power flow and phase velocity are directed from the laser side to the CPA side, and negative refraction can be obtained without the need for

a bulk negative refractive index material [5,16]. With the study of PT-symmetric systems, it has been found that the imaginary part of the material parameters representing the loss and gain of materials plays an important role in the modulation of the wave field [5,16,18–22].

In recent years, purely imaginary metamaterials (PIMs) were originally proposed in the field of optics [23–27], and since both light and sound are classical waves, similar materials were introduced into the field of acoustics [28–30]. Unlike the spatially distributed loss and gain in PT-symmetric systems, PIM has balanced loss and gain uniformly distributed in space, but in different material parameters. It is worth noting that CPA mode and laser mode can also be implemented in acoustic PIM structures [28–30]. Yet, they usually occur in different cases. That is, for a given PIM slab, the CPA mode and the laser mode have different wave vectors and cannot be excited at the same angle of incidence. To solve this problem, the acoustic CPA mode is usually obtained from a PIM slab, while the acoustic laser mode is implemented on another PIM slab with conjugate material parameters [28]. However, the negative refraction achieved using this structure has a requirement for the direction of incidence, i.e., the beam can only be incident from the CPA side.

In this work, analytical solutions have been derived for the coexistence of acoustic CPA mode and acoustic laser mode in a single PIM slab. Such PIM slabs can freely switch states between the acoustic coherent perfect absorption and the acoustic laser depending on the direction of incidence. Further, by using a pair of identical PIM slabs, bidirectional negative refraction and planar focusing can be achieved. In this process, the illuminated PIM slab operates as a coherent perfect absorber, completely absorbing the incident wave, while the other identical PIM slab operates in the mode of a coherent laser, reproducing the incident acoustic waves on both sides. Moreover, the parameters in the appropriate range can be found by adjusting the mode order, which facilitates the experimental verification. To date, the required acoustically pure imaginary metamaterial (PIM) has not been experimentally demonstrated, so the results presented in the manuscript are theoretical speculations on its existence.

2. Derivation of Coexistence Conditions for CPA and Laser Modes in a Single Acoustic PIM Slab

Figure 1 illustrates the structure under study. A PIM slab of thickness d is sandwiched between two semi-infinite background layers. Without loss of generality, the background material is set to be air with a mass density of $\rho_0 = 1.21 \, \text{kg/m}^3$ and a velocity of $c_0 = 343 \, \text{m/s}$. In terms of PIM material parameters, both bulk compressibility $\beta_s = i\beta_r\beta_0$ and mass density $\rho = -i\rho_r\rho_0$ are purely imaginary numbers with conjugate phase factors, where β_0 and ρ_0 are the corresponding parameters of air, and β_r and ρ_r are relative parameters which are real numbers. It can be found that the speed of sound $c = \pm\sqrt{(\rho\beta_s)^{-1}}$ and the refractive index $n = \pm\sqrt{\rho\beta_s/\rho_0\beta_0}$ are real numbers. The blue rays indicate the incident waves, while the black and red rays indicate the scattered waves in the PIM slab and the background medium, respectively.

Due to the opposite sign of the imaginary part of the bulk compressibility and mass density, the material of PIM contains both gain and loss elements. If the gain element dominates, the incident wave may excite the transmitted and reflected waves so strongly that the injected waves can be ignored. This corresponds to the acoustic laser mode, as shown in Figure 1a. In contrast, if the loss element dominates, the coherent waves incident from both sides can be completely absorbed by the PIM slab without any scattered waves. This is equivalent to the CPA mode, as shown in Figure 1b.
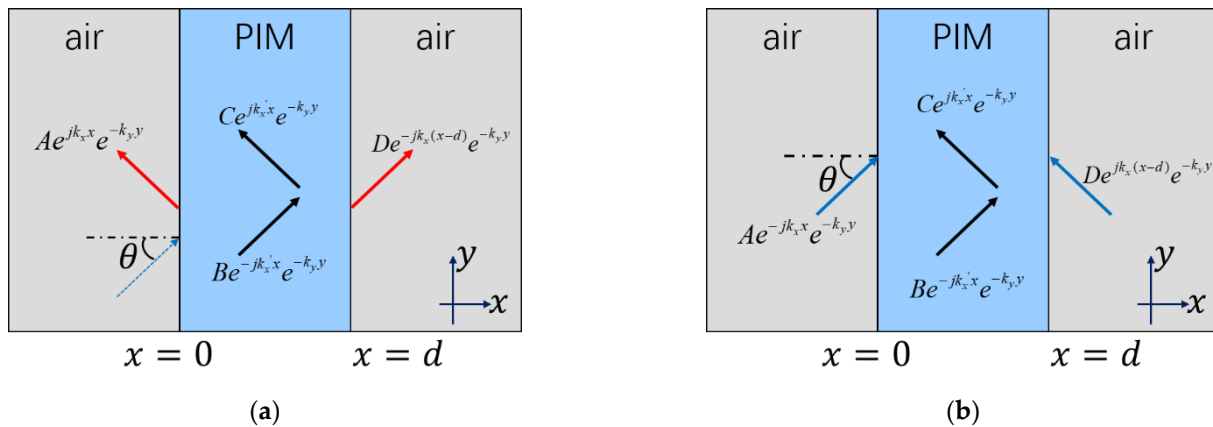
Figure 1. Sketch of the scattering process of (**a**) laser and (**b**) CPA modes in PIM slabs. The blue rays indicate the incident waves, while the black and red rays indicate the scattered waves in the PIM slab and background medium, respectively.

By analyzing the scattering characteristics of the PIM slab with thickness of d in air, combined with the boundary conditions, the dispersion relation of the acoustic laser mode can be ascribed as

$$\left(\frac{1-\eta}{1+\eta}\right)^2 = e^{j2k_x'd}. \tag{1}$$

Correspondingly, the dispersion relation for the acoustic CPA mode is

$$\left(\frac{1-\eta}{1+\eta}\right)^2 = e^{-j2k_x'd}. \tag{2}$$

Here, $k_0 = 2\pi/\lambda$ is the wave vector in air, $\eta = \rho k_x / \rho_0 k_x'$ is the relative impedance of the PIM-air interface, and $k_x = \sqrt{k_0^2 - k_y^2}$, $k_x' = \sqrt{n'^2 k_0^2 - k_y^2}$ are the x directional wave vector in the air and PIM media, respectively. (For detailed derivation, see Appendix A).

By comparing Equations (1) and (2), it can be found that in general, the laser mode and the CPA mode appear in different situations. That is, for given material parameters, the laser mode and the CPA mode have different wave vectors. However, when $\left(\frac{1-\eta}{1+\eta}\right)^2 = e^{j2k_x'd} = e^{-j2k_x'd}$, the CPA mode and the laser mode can be satisfied simultaneously. After further solving, we can get two sets of analytical solutions, which are

$$\begin{cases} \rho_r = \sqrt{\dfrac{\frac{\pi^2}{k_0^2 d^2}\left(2m+\frac{1}{2}\right)^2}{(1-\sin^2\theta)}} = \frac{\pi}{k_0 d} \times \left(2m+\frac{1}{2}\right)/\cos\theta \\ \beta_r = \left[\frac{\pi^2}{k_0^2 d^2}\left(2m+\frac{1}{2}\right)^2 + \sin^2\theta\right]/\left[\frac{\pi}{k_0 d} \times \left(2m+\frac{1}{2}\right)/\cos\theta\right] \end{cases} \tag{3}$$

and

$$\begin{cases} \rho_r = \sqrt{\dfrac{\frac{\pi^2}{k_0^2 d^2}\left(2m+\frac{1}{2}\right)^2}{(1-\sin^2\theta)}} = \frac{\pi}{k_0 d} \times \left(2m-\frac{1}{2}\right)/\cos\theta \\ \beta_r = \left[\frac{\pi^2}{k_0^2 d^2}\left(2m-\frac{1}{2}\right)^2 + \sin^2\theta\right]/\left[\frac{\pi}{k_0 d} \times \left(2m-\frac{1}{2}\right)/\cos\theta\right] \end{cases}. \tag{4}$$

Here, m is an arbitrary integer related to the mode order. (For detailed derivation, see Appendix B).

Based on the above analytical results, further numerical simulations of the coexistence of the laser mode and the CPA mode were carried out using COMSOL Multiphysics software (version 4.2). Without loss of generality, the width of the PIM slab is set to 2λ and the black vertical lines indicate the outer boundary of the PIM slab. As a periodic boundary condition is set in the y-direction, the height of the PIM slab does not affect the

acoustic field distribution, which is set to 4λ in the following simulations. A plane wave radiation boundary is imposed on the incident and transmitted boundaries. The incident angle is set to be $20°$ and the black arrows in Figure 2 indicate the direction of energy flow in each region.
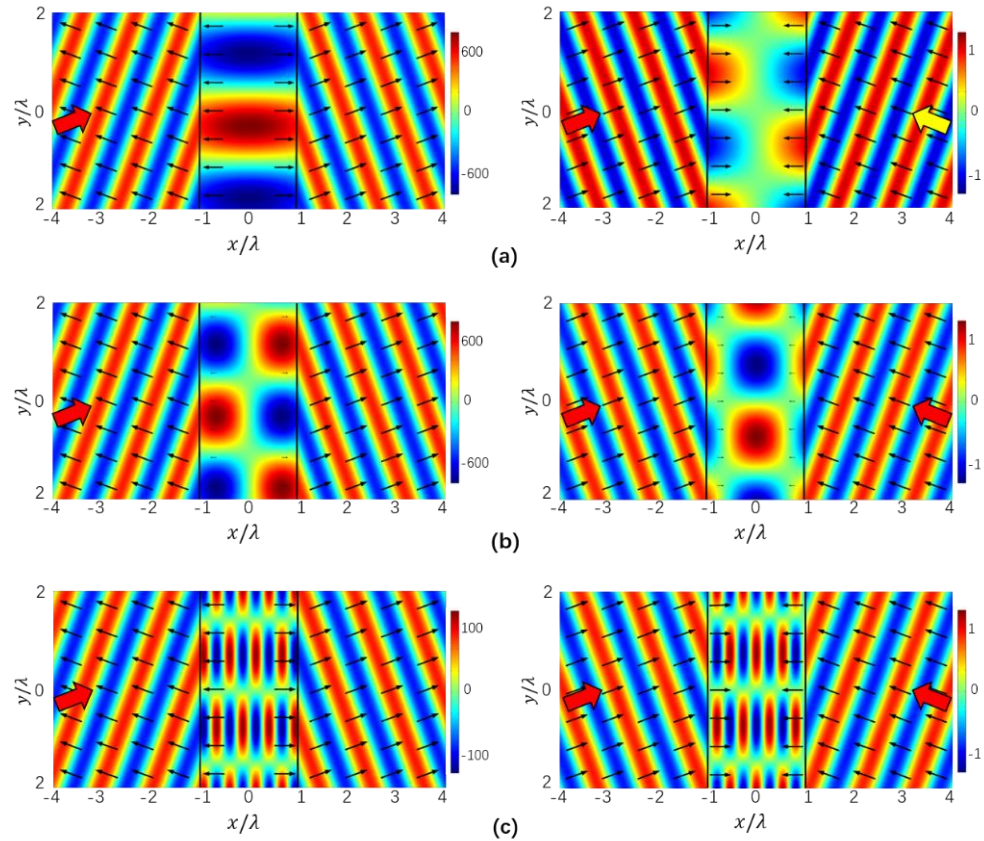

Figure 2. The simulated acoustic fields for laser modes (**left** panels) and CPA modes (**right** panels). The parameters in (**a**) are $\rho_r = 0.13$ and $\beta_r = 1.00$, in (**b**) are $\rho_r = 0.40$ and $\beta_r = 0.65$, and in (**c**) are $\rho_r = 1.99$ and $\beta_r = 1.82$. In all simulations, the incident wavelength is λ, the width of the PIM slab is $d = 2\lambda$, the incident amplitude is 1 Pa, and the incident angle is set to be $20°$.

According to Equation (3), when the *m* is taken as zero, the density obtained is 0.13 and the bulk compressibility is 1.00. The left panel of Figure 2a shows the total acoustic field pattern when a plane wave is incident from the left side at an incident angle of $20°$, as shown by the red arrow. The total field far exceeds the intensity of the incident field (refer to the color bar) and the distribution is symmetric about the line $x = 0$. Thus, this is consistent with the distribution pattern of the even acoustic laser mode. The right panel of Figure 2a gives the acoustic field distribution when two waves of opposite phase are incident from the left and right sides with the identical angle indicated by the red and yellow arrows, respectively. The absence of any acoustic scattering in the background media indicates that the coherent incident waves are completely absorbed in the PIM slab structure by the effect of interference as well as material absorption. Additionally, the results show that the amplitude distribution is asymmetric with respect to the line $x = 0$. Therefore, an odd CPA mode can also be excited with the same structure and material parameters. Similarly, when taking *m* as one in Equation (4), we can obtain a density of 0.40 and a bulk compressibility of 0.65. The two panels of Figure 2b show the total acoustic pressure field when one wave is incident from the left and when two waves are incident in phase from both sides, respectively. By observing the field patterns and the direction of the energy flow indicated by the black arrows, it could be found that odd laser modes and even CPA modes can be excited. To investigate the role played by the parameter *m* in

the equations, the other terms are kept the same and the parameter m in Equation (4) is changed from one to four. The coefficients obtained are $\rho_r = 1.99$ and $\beta_r = 1.82$. Similar to the cases of Figure 2b, the odd laser mode and the even CPA mode are successfully excited as shown in Figure 2c. The difference is that the mode of the PIM slab in Figure 2c is three orders higher due to the change of m from one to four.

The simulation results in Figure 2 confirm that even laser modes and odd CPA modes are supported when the acoustic parameters conform to Equation (3), while odd laser modes and even CPA modes can be achieved when the acoustic parameters conform to Equation (4). The integer m determines the order of the modes in the PIM slab and can be used to adjust the material parameters to a range suitable for experimental implementation.

3. Bidirectional Negative Refraction

In the previous section, we showed that the coexistence of CPA mode and laser mode can be achieved using a PIM slab with specific acoustic parameters. When the thickness and acoustic material parameters of the PIM slab satisfy Equation (3), even laser mode and odd CPA mode can be supported; when the thickness and acoustic material parameters of the PIM slab satisfy Equation (4), even CPA mode and odd laser mode can be supported. The coexistence of modes provides the possibility of negative refraction with a pair of identical PIM slabs.

As sketched in Figure 3a, the structure consists of two PIM slabs separated by a distance L in air. The relationship between the transmission and reflection coefficients of the system with the incident angle θ and spacing L can be obtained by calculating the elements of the scatting matrix of the system [28]. When the acoustic material parameters of the PIM slab satisfy Equation (3) or Equation (4), the calculated results are shown in Figure 3b,c, respectively. It can be found that in this matched case, the amplitude of reflectance is in the order of 10^{-15} and the logarithm of the amplitude of the transmittance is in the order of 10^{-16}. Therefore, the reflection coefficient is almost zero, while the transmission coefficient is very close to the unity. Both are essentially independent of the incident angle and the spacing. Therefore, omnidirectional negative refraction can be achieved and is independent of the spacing between the two PIM slabs.
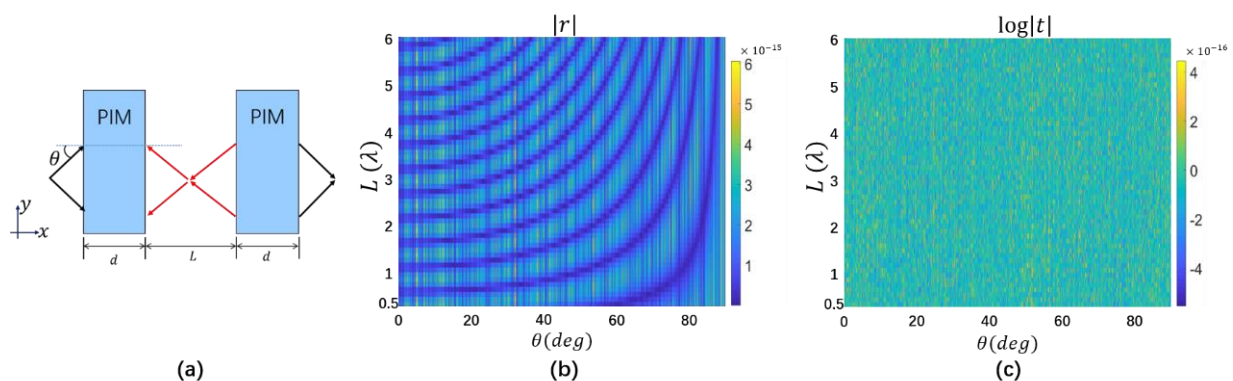

Figure 3. (**a**) Schematic diagram of negative refraction based on two identical PIM slabs. (**b**)The magnitude of the transmission coefficient and (**c**) the logarithm of the amplitude of the transmittance coefficient as a function of the angle of incidence θ and the spacing L between the two slabs.

Numerical simulations were performed using the finite element method to verify the theoretical analysis results. As shown in Figure 4, two identical PIM slabs with width 2λ are immersed in the air and the four black vertical lines indicate the outer boundaries of the left and right PIM slabs, respectively. The incidence angle is arbitrarily taken as $30°$. The black arrows indicate the direction of the energy flow in each region.
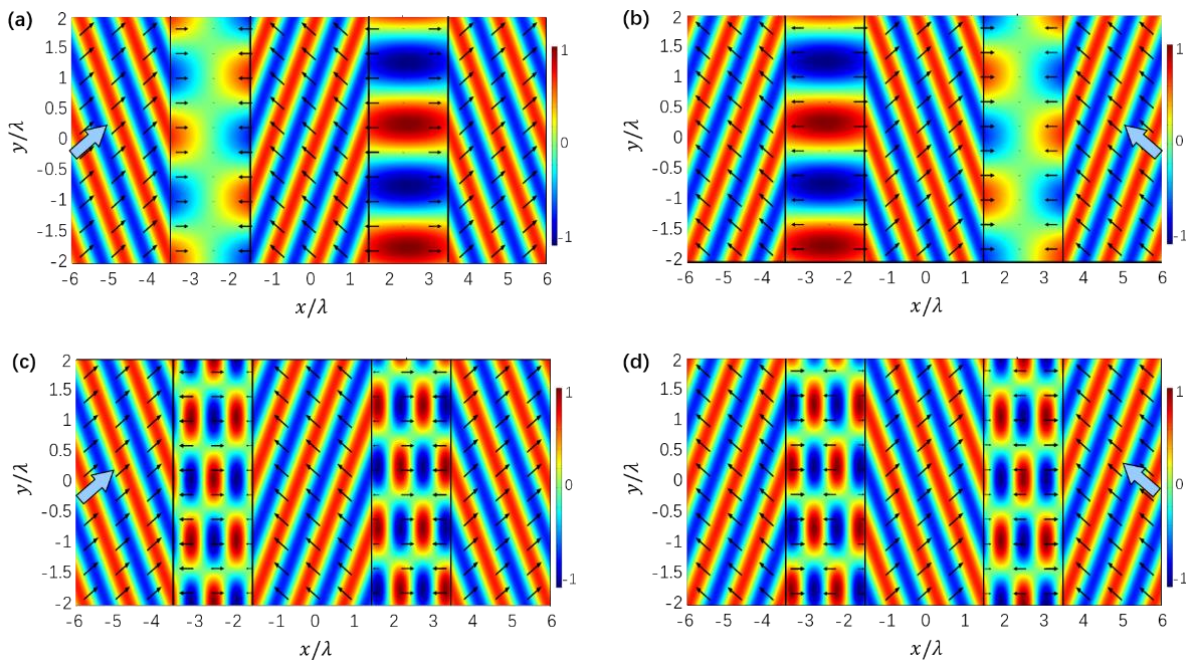
Figure 4. The simulated acoustic field patterns for negative using a pair of identical PIMs supporting the coexistence of CPA and laser modes. (**a**,**b**) are the simulated acoustic field patterns when the waves are incident from the left and right sides, respectively. The relative coefficients are $\rho_r = 0.14$ and $\beta_r = 1.84$. (**c**,**d**) are the simulated acoustic field pattern for the incident waves from the left and right sides, respectively. The relative coefficients are $\rho_r = 1.01$ and $\beta_r = 1.01$.

In Figure 4a,b, the density and the bulk compressibility of the PIM slab are $\rho_r = 0.14$ and $\beta_r = 1.84$, respectively. The material parameters are calculated using Equation (3) with m taken as zero, which supports the coexistence of even laser mode and odd CPA mode. While in Figure 4c,d, the density $\rho_r = 1.01$ and the bulk compressibility $\beta_r = 1.01$ are calculated using Equation (4) with m taken as two and the coexistence of odd laser mode and even CPA mode are supported. The simulation results in Figure 4 show that in all four cases, the amplitude of total acoustic pressure field in the background medium is equal to that of the incident field (see color bar) and there is no significant scattering.

When the acoustic wave is incident from the left shown by the blue arrows, it can be seen from Figure 4a,c that a backward energy flow occurs in the air between the two slabs, forming a negative refraction. The backward wave in the air gap forms a CPA mode with the incident wave on the first PIM slab and a laser mode with the transmitted wave on the second PIM slab. Similarly, as shown in Figure 4b,d, the incident acoustic wave from the right side indicated by the blue arrows also generates a reverse energy flow in the air between the two slabs, which together with the incident acoustic wave constitutes the CPA mode and together with the transmitted acoustic wave constitutes the laser mode.

The discussion of mode polarity in the PIM slab is the same as in the previous section. For example, in Figure 4a,b, the parameters of the PIM slabs are calculated by Equation (3), and the even laser mode and the odd CPA mode are obtained; while in Figure 4c,d, the parameters of PIM slabs are calculated by Equation (4), and the odd laser mode and even the CPA mode are excited. In this process, the illuminated PIM slab works as a coherent perfect absorber, completely absorbing the incident wave, while the other part works in a coherent laser mode, reproducing the incident wave on both sides.

The previous section shows how acoustic negative refraction can be achieved using a pair of identical PIM slabs. However, plane waves are an idealization. In practice, waves are non-planar in nature because they are generated by a finite number of sources, such as antennas. Fortunately, non-planar waves can be expanded into plane waves based on the

Fourier transform. In the following, we will further implement flat plate focusing based on the negative refraction of plane waves.

Take two PIM slabs with a thickness of 0.3λ and a spacing of 12λ as an example, the focal length is set to 6λ, then the relationship between the y-coordinate and the incident angle is $\theta = arc\tan(y/6\lambda)$. In the case of coexistence of CPA and Laser modes, the required material parameters can be acquired by Equation (3) or Equation (4). In Equation (3), we arbitrarily choose to take the m as zero to obtain a set of material parameters as shown in Figure 1a.

The point sources are placed at $(-12r, 0)$ and $(12r, 0)$, respectively. Figure 5b,d show the simulated pressure field pattern under point sources located at the left and right sides, respectively. As expected, in both cases, two focal points appear between the slabs and on the other side of the source, respectively. The red and black curves in Figure 5c represent the intensity fields in the focal planes shown in Figure 5b,d, respectively. The width of the focal point as well as the field distribution confirm that the proposed structure can ideally focus the propagating spectrum. Bidirectional diffraction-limited planar focusing is possible. It should be noted that the source point and the two image points are coherent. The illuminated PIM slab operates in CPA mode, so the symmetry of the field distribution on both sides of it is determined by the polarity of the CPA mode; while the other PIM slab works in laser mode and its polarity also determines whether the fields on both sides are in-phase or out of phase.
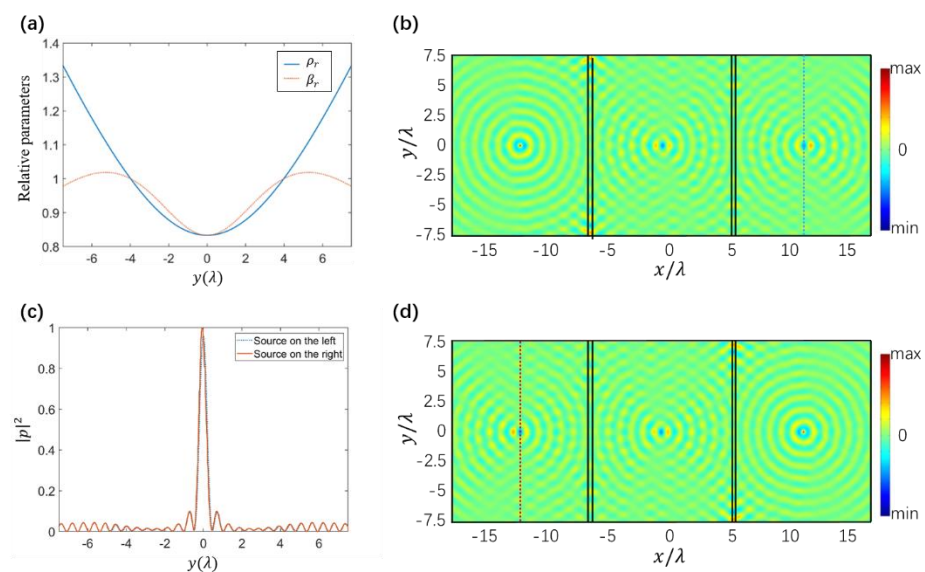

Figure 5. (**a**) The relative material parameters ρ_r and β_r versus y-coordinate. (**b,d**) the acoustic field patterned with point source placed at $(-12r, 0)$ and $(12r, 0)$, respectively. (**c**) The acoustic field intensity amplitudes at the imaging planes. The red and black curves represent the intensity fields in the focus planes indicated by the red dashed lines in (**b,d**), respectively.

4. Discussion and Conclusions

It is worth noting that when the laser mode is implemented, the energy of the transmitted and reflected waves is greater than the energy of the incident waves, so this mode generates energy, or to put it another way, requires energy input. The input of energy can be achieved by means of acoustic gain media. The imaginary part of the material parameters represents the loss and gain of the material. Thus, due to the opposite sign of the imaginary part of the bulk compressibility and mass density, the material of the PIM slabs contains both gain and loss elements.

At present, the experimental research of acoustic PIM system is still in the early stage. A major challenge lies in the design and implementation of acoustic gain media. Loudspeakers with appropriate gain circuitry [20,31] or acoustoelectric effects using piezo-

electric semiconductors [32,33] have been widely used to provide wave amplification in experiments, despite the complex circuitry and external energy involved. Due to the low heat capacitance and thermal inertia of carbon nanotubes (CNTs), a more flexible and tunable approach is proposed by employing thermoacoustics, where the fluctuating Joule heating is converted to sound [34–36]. So far, PIM systems have mostly been discussed theoretically [25–28,30]. Therefore, practical applications in this work may require further sophisticated design and engineering.

In conclusion, we have derived the explicit expressions of material parameters required for the coexistence of laser and CPA modes in the acoustic PIM slab. Numerical simulations confirm that coexistence of odd laser and even CPA modes or coexistence of even laser and odd CPA modes can be achieved with different orders. Such a PIM slab can freely switch states between coherent complete absorber and acoustic laser depending on the direction of incidence. We further demonstrate that planar focusing can be achieved with gradient refractive index materials. These findings may find applications in acoustic amplification, absorption and imaging. In addition, the parameters in the appropriate range can be found by adjusting the mode order, which facilitates experimental verification. So far, the required acoustically pure imaginary metamaterial (PIM) has not been experimentally demonstrated, so the results presented in the manuscript are theoretical speculations on its existence.

Author Contributions: Conceptualization, L.-L.Z. and X.-J.L.; funding acquisition, L.-L.Z., Y.J., P.C., Q.D. and X.-J.L.; investigation, L.-L.Z., Y.J., P.C., Q.D. and X.-J.L.; project administration, L.-L.Z. and X.-J.L.; writing—original draft, L.-L.Z.; writing—review and editing, L.-L.Z. and X.-J.L. All authors have read and agreed to the published version of the manuscript.

Institutional Review Board Statement: Not applicable.

Informed Consent Statement: Not applicable.

Conflicts of Interest: The authors declare no conflict of interest.

Appendix A

Appendix A.1. Scattering Process of Acoustic Laser Mode

For the acoustic laser mode, the incident wave can be neglected because the outgoing wave is strong and the corresponding scattering process is shown in Figure 1a. The distribution of the acoustic field in different regions is,

$$
\begin{cases}
p_1 = A e^{jk_x x} e^{-jk_y y} & (x < 0) \\
p_2 = \left(B e^{-jk_x' x} + C e^{jk_x' x} \right) e^{-jk_y y} & (0 < x < d). \\
p_3 = D e^{-jk_x(x-d)} e^{-jk_y y} & (x > d)
\end{cases}
\tag{A1}
$$

And the relationship between velocity and acoustic pressure is given by $v = -\frac{1}{\rho} \int \nabla p \, dt$. Assuming the $e^{j\omega t}$ convention, the expressions of the acoustic velocity in each regions are give by

$$
\begin{cases}
\vec{v_1} = [-\frac{k_x}{\omega\rho_0}\vec{e_x} + \frac{k_y}{\omega\rho_0}\vec{e_y}] A e^{jk_x x} e^{-jk_y y} & (x < 0) \\
\vec{v_2} = [\frac{k_x'}{\omega\rho_1}\vec{e_x} + \frac{k_y}{\omega\rho_1}\vec{e_y}] B e^{-jk_x' x} e^{-jk_y y} + [\frac{-k_x'}{\omega\rho_1}\vec{e_x} + \frac{k_y}{\omega\rho_1}\vec{e_y}] C e^{jk_x' x} e^{-jk_y y} & (0 < x < d). \\
\vec{v_3} = [\frac{k_x}{\omega\rho_0}\vec{e_x} + \frac{k_y}{\omega\rho_0}\vec{e_y}] D e^{-jk_x(x-d)} e^{-jk_y y} & (x > d)
\end{cases}
\tag{A2}
$$

The acoustic pressure and normal velocity are continuous at the interface of two different media. So, according to the boundary conditions at $x = 0$ and $x = d$, we can obtain the following equations,

$$
\begin{cases}
A = B + C \\
A\frac{-k_x}{\rho_0} = B\frac{k_x'}{\rho'} - C\frac{k_x'}{\rho'} \\
Be^{-jk_x'd} + Ce^{jk_x'd} = D \\
\frac{k_x'}{\rho'}Be^{-jk_x'd} + \frac{-k_x'}{\rho'}Ce^{jk_x'd} = \frac{k_x}{\rho_0}D
\end{cases}
. \tag{A3}
$$

After further simplification and taking $\eta = \frac{k_x}{\rho_0} / \frac{k_x'}{\rho'} = \frac{\rho'k_x}{\rho_0 k_x'}$, the dispersion relation for the laser mode can be obtained as

$$
\left(\frac{1-\eta}{1+\eta}\right)^2 = \frac{e^{jk_x'd}}{e^{-jk_x'd}}. \tag{A4}
$$

Appendix A.2. Scattering Process of the Acoustic CPA Mode

As shown in Figure 1b, for the acoustic CPA mode, the outgoing waves can be neglected, i.e., the outgoing waves are zero. The acoustic field distribution of the corresponding area is expressed as,

$$
\begin{cases}
p_1 = Ae^{-jk_xx}e^{-jk_yy} & (x < 0) \\
p_2 = \left(Be^{-jk_x'x} + Ce^{jk_x'x}\right)e^{-jk_yy} & (0 < x < d). \\
p_3 = De^{jk_x(x-d)}e^{-jk_yy} & (x > d)
\end{cases}
\tag{A5}
$$

According to the relationship between velocity and acoustic pressure $v = -\frac{1}{\rho}\int \nabla p\, dt$, the following equations can be obtained,

$$
\begin{cases}
\vec{v_1} = [\frac{k_x}{\omega\rho_0}\vec{e_x} + \frac{k_y}{\omega\rho_0}\vec{e_y}]Ae^{-jk_xx}e^{-jk_yy} & (x < 0) \\
\vec{v_2} = [\frac{k_x'}{\omega\rho_1}\vec{e_x} + \frac{k_y}{\omega\rho_1}\vec{e_y}]Be^{-jk_x'x}e^{-jk_yy} + [\frac{-k_x'}{\omega\rho_1}\vec{e_x} + \frac{k_y}{\omega\rho_1}\vec{e_y}]Ce^{jk_x'x}e^{-jk_yy} & (0 < x < d). \\
\vec{v_3} = [\frac{-k_x}{\omega\rho_0}\vec{e_x} + \frac{k_y}{\omega\rho_0}\vec{e_y}]De^{jk_x(x-d)}e^{-jk_yy} & (x > d)
\end{cases}
\tag{A6}
$$

By matching the boundary conditions at $x = 0$, d, we get

$$
\begin{cases}
A = B + C \\
A\frac{k_x}{\rho_0} = B\frac{k_x'}{\rho'} - C\frac{k_x'}{\rho'} \\
Be^{-jk_x'd} + Ce^{jk_x'd} = D \\
\frac{k_x'}{\rho'}Be^{-jk_x'd} + \frac{-k_x'}{\rho'}Ce^{jk_x'd} = \frac{-k_x}{\rho_0}D
\end{cases}
. \tag{A7}
$$

Let $\eta = \frac{k_x}{\rho_0} / \frac{k_x'}{\rho'} = \frac{\rho'k_x}{\rho_0 k_x'}$, the dispersion relation for the CPA mode can be solved as

$$
\left(\frac{1-\eta}{1+\eta}\right)^2 = \frac{e^{-jk_x'd}}{e^{jk_x'd}}. \tag{A8}
$$

Appendix B

We focus on the scattering properties of a PIM slab with thickness of d in air, as shown in Figure 1. Consider monochromatic acoustic waves with frequency ω and incident angle θ. As discussed in the previous section, the dispersion relations of acoustic laser mode and CPA mode can be expressed as $\left(\frac{1-\eta}{1+\eta}\right)^2 = e^{j2k_x'd}$ and $\left(\frac{1-\eta}{1+\eta}\right)^2 = e^{-j2k_x'd}$, respectively.

In general, these two modes appear in different situations. However, when $\left(\frac{1-\eta}{1+\eta}\right)^2 = e^{j2k_x{}'d} = e^{-j2k_x{}'d}$, i.e., when $\frac{e^{jk_x{}'d}}{e^{-jk_x{}'d}} = \pm 1$, the CPA mode and the laser mode can be satisfied simultaneously.

If $\frac{e^{jk_x{}'d}}{e^{-jk_x{}'d}} = 1$ holds, we can get $\eta = 0$. This indicates that the wave vector in the x-direction is zero, i.e., the wave cannot propagate forward in the air, so this solution can be ignored. And if $\frac{e^{jk_x{}'d}}{e^{-jk_x{}'d}} = -1$ holds, we can get $\eta = -i$ and $e^{ik_x'd} = \pm i$.

Case 1: $e^{ik_x'd} = i$

For $e^{ik_x'd} = i$, the result $k_x'd = (2m + \frac{1}{2})\pi$ can be derived, where, m is an arbitrary integer related to the mode order. And since $\eta = \frac{\rho k_x}{\rho_0 k_x{}'} = \frac{-i\rho_r\rho_0 k_x}{\rho_0 k_x{}'} = \frac{-i\rho_r k_x}{k_x{}'} = -i$, we can get $\frac{\rho k_x}{k_x{}'} = 1$. Thus, the problem is transformed into solving the following set of equations,

$$
\begin{cases}
\frac{\rho k_x}{k_x{}'} = 1 \\
k_x'd = (2m + \frac{1}{2})\pi
\end{cases},
\tag{A9}
$$

where $k_y = k_0 \sin\theta$ is the wave vector along the y directions, and $k_x = \sqrt{k_0{}^2 - k_y{}^2}$, $k_x' = \sqrt{n'^2 k_0{}^2 - k_y{}^2}$ are the x directional wave vector in the air and PIM media, respectively. $n = \pm\sqrt{\rho\beta_s/\rho_0\beta_0} = \pm\sqrt{\rho_r\beta_r}$ is the refractive index. The solution of Equation (A9) is as follows:

$$
\begin{cases}
\rho_r = \sqrt{\frac{\frac{\pi^2}{k_0{}^2 d^2}(2m+\frac{1}{2})^2}{(1-\sin^2\theta)}} = \frac{\pi}{k_0 d} \times (2m + \frac{1}{2}) / \cos\theta \\
\beta_r = [\frac{\pi^2}{k_0{}^2 d^2}(2m + \frac{1}{2})^2 + \sin^2\theta] / [\frac{\pi}{k_0 d} \times (2m + \frac{1}{2}) / \cos\theta]
\end{cases}.
\tag{A10}
$$

Case 2: $e^{ik_x'd} = -i$

Similarly, for $e^{ik_x'd} = -i$, the result $k_x'd = (2m - \frac{1}{2})\pi$ can be derived. Combined with $\eta = \frac{\rho k_x}{\rho_0 k_x{}'} = \frac{-i\rho_r\rho_0 k_x}{\rho_0 k_x{}'} = \frac{-i\rho_r k_x}{k_x{}'} = -i$, i.e., $\frac{\rho k_x}{k_x{}'} = 1$. The problem is transformed into solving the following set of equations,

$$
\begin{cases}
\frac{\rho k_x}{k_x{}'} = 1 \\
k_x'd = (2m - \frac{1}{2})\pi
\end{cases}
\tag{A11}
$$

The parameters are set in the same way as in case 1. The solution of Equation (A11) is

$$
\begin{cases}
\rho_r = \sqrt{\frac{\frac{\pi^2}{k_0{}^2 d^2}(2m+\frac{1}{2})^2}{(1-\sin^2\theta)}} = \frac{\pi}{k_0 d} \times (2m - \frac{1}{2}) / \cos\theta \\
\beta_r = [\frac{\pi^2}{k_0{}^2 d^2}(2m - \frac{1}{2})^2 + \sin^2\theta] / [\frac{\pi}{k_0 d} \times (2m - \frac{1}{2}) / \cos\theta]
\end{cases}.
\tag{A12}
$$

References

1. Veselago, V.G. Electrodynamics of substances with simultaneously negative values of sigma and mu. *Sov. Phys. Uspekhi-Ussr* **1968**, *10*, 509. [CrossRef]
2. McCall, M.W. What is negative refraction? *J. Mod. Opt.* **2009**, *56*, 1727–1740. [CrossRef]
3. Zhang, Y.; Mascarenhas, A. Total and negative refraction of electromagnetic waves. *Mod. Phys. Lett. B* **2005**, *19*, 21–33. [CrossRef]
4. Pendry, J.B. Negative refraction makes a perfect lens. *Phys. Rev. Lett.* **2000**, *85*, 3966–3969. [CrossRef]
5. Fleury, R.; Sounas, D.L.; Alu, A. Negative Refraction and Planar Focusing Based on Parity-Time Symmetric Metasurfaces. *Phys. Rev. Lett.* **2014**, *113*, 023903. [CrossRef]
6. Pendry, J.B. Negative refraction. *Contemp. Phys.* **2004**, *45*, 191–202. [CrossRef]
7. Shelby, R.A.; Smith, D.R.; Schultz, S. Experimental verification of a negative index of refraction. *Science* **2001**, *292*, 77–79. [CrossRef]
8. Smith, D.R.; Kroll, N. Negative refractive index in left-handed materials. *Phys. Rev. Lett.* **2000**, *85*, 2933–2936. [CrossRef]
9. Li, J.; Chan, C.T. Double-negative acoustic metamaterial. *Phys. Rev. E* **2004**, *70*, 055602. [CrossRef]
10. Maslovski, S.; Tretyakov, S. Phase conjugation and perfect lensing. *J. Appl. Phys.* **2003**, *94*, 4241–4243. [CrossRef]

11. Maslovski, S.; Tretyakov, S. Perfect lensing with phase-conjugating surfaces: Toward practical realization. *New J. Phys.* **2012**, *14*, 035007. [CrossRef]

12. He, H.; Qiu, C.; Ye, L.; Cai, X.; Fan, X.; Ke, M.; Zhang, F.; Liu, Z. Topological negative refraction of surface acoustic waves in a Weyl phononic crystal. *Nature* **2018**, *560*, 61–64. [CrossRef] [PubMed]

13. Liu, J.; Guo, H.; Wang, T. A Review of Acoustic Metamaterials and Phononic Crystals. *Crystals* **2020**, *10*, 305. [CrossRef]

14. Nemat-Nasser, S. Inherent negative refraction on acoustic branch of two dimensional phononic crystals. *Mech. Mater.* **2019**, *132*, 1–8. [CrossRef]

15. Danawe, H.; Tol, S. Experimental realization of negative refraction and subwavelength for flexural waves in. *J. Sound Vib.* **2022**, *518*, 116552. [CrossRef]

16. Monticone, F.; Valagiannopoulos, C.A.; Alu, A. Parity-Time Symmetric Nonlocal Metasurfaces: All-Angle Negative Refraction and Volumetric Imaging. *Phys. Rev. X* **2016**, *6*, 041018. [CrossRef]

17. Lan, J.; Zhang, X.; Wang, L.; Lai, Y.; Liu, X. Bidirectional acoustic negative refraction based on a pair of metasurfaces with both local and global PT-symmetries. *Sci. Rep.* **2020**, *10*, 10794. [CrossRef]

18. Peng, B.; Oezdemir, S.K.; Lei, F.; Monifi, F.; Gianfreda, M.; Long, G.L.; Fan, S.; Nori, F.; Bender, C.M.; Yang, L. Parity-time-symmetric whispering-gallery microcavities. *Nat. Phys.* **2014**, *10*, 394–398. [CrossRef]

19. Ozdemir, S.K.; Rotter, S.; Nori, F.; Yang, L. Parity-time symmetry and exceptional points in photonics. *Nat. Mater.* **2019**, *18*, 783–798. [CrossRef]

20. Fleury, R.; Sounas, D.; Alu, A. An invisible acoustic sensor based on parity-time symmetry. *Nat. Commun.* **2015**, *6*, 5905. [CrossRef]

21. Hu, T.; Wei, Q.; Zhu, X.-F.; Yao, J.; Wu, D.-J. Acoustic anti-parity-time symmetric structure enabling equivalent lasing and coherent perfect absorption. *Phys. Rev. B* **2021**, *104*, 134110. [CrossRef]

22. Valagiannopoulos, C.A.; Monticone, F.; Alu, A. PT-symmetric planar devices for field transformation and imaging. *J. Opt.* **2016**, *18*, 044028. [CrossRef]

23. Xu, Y.; Fu, Y.; Chen, H. Electromagnetic wave propagations in conjugate metamaterials. *Opt. Express* **2017**, *25*, 4952–4966. [CrossRef] [PubMed]

24. Dragoman, D. Complex conjugate media: Alternative configurations for miniaturized lasers. *Opt. Commun.* **2011**, *284*, 2095–2098. [CrossRef]

25. Fu, Y.-Y.; Xu, Y.-D.; Chen, H.-Y. Negative refraction based on purely imaginary metamaterials. *Front. Phys.* **2018**, *13*, 134206. [CrossRef]

26. Tao, J.; Liu, J.; Dong, D.; Liu, Y.; Fu, Y. Extraordinary wave modes in purely imaginary metamaterials beyond the critical angle. *Opt. Express* **2021**, *29*, 2874–2883. [CrossRef]

27. Fu, Y.; Cao, Y.; Cummer, S.A.; Xu, Y.; Chen, H. Coherent perfect absorber and laser modes in purely imaginary metamaterials. *Phys. Rev. A* **2017**, *96*, 043838. [CrossRef]

28. Zhang, L.-L.; Liu, X.-J. Acoustic Negative Refraction and Planar Focusing Based on Purely Imaginary Metamaterials. *Appl. Sci.* **2022**, *12*, 5962. [CrossRef]

29. Ma, X.-X.; Wei, Q.; Zhu, X.-F.; Yao, J.; Wu, D.-J. Acoustic Equivalent Lasing and Coherent Perfect Absorption Based on a Conjugate Metamaterial Sphere. *Appl. Sci.* **2022**, *12*, 1777. [CrossRef]

30. Chen, L.; Fan, L.; Zhang, S.-Y. Acoustic conjugate metamaterials. *Phys. Rev. B* **2019**, *100*, 024111. [CrossRef]

31. Shi, C.; Dubois, M.; Chen, Y.; Cheng, L.; Ramezani, H.; Wang, Y.; Zhang, X. Accessing the exceptional points of parity-time symmetric acoustics. *Nat. Commun.* **2016**, *7*, 11110. [CrossRef] [PubMed]

32. Popa, B.-I.; Cummer, S.A. Non-reciprocal and highly nonlinear active acoustic metamaterials. *Nat. Commun.* **2014**, *5*, 3398. [CrossRef] [PubMed]

33. Hutson, A.R.; White, D.L.; McFee, J.H. Ultrasonic Amplification in CDS. *Phys. Rev. Lett.* **1961**, *7*, 237. [CrossRef]

34. Xiao, L.; Chen, Z.; Feng, C.; Liu, L.; Bai, Z.-Q.; Wang, Y.; Qian, L.; Zhang, Y.; Li, Q.; Jiang, K.; et al. Flexible, Stretchable, Transparent Carbon Nanotube Thin Film Loudspeakers. *Nano Lett.* **2008**, *8*, 4539–4545. [CrossRef] [PubMed]

35. Aliev, A.E.; Lima, M.D.; Fang, S.; Baughman, R.H. Underwater Sound Generation Using Carbon Nanotube Projectors. *Nano Lett.* **2010**, *10*, 2374–2380. [CrossRef]

36. Hu, B.; Zhang, Z.; Zhang, H.; Zheng, L.; Xiong, W.; Yue, Z.; Wang, X.; Xu, J.; Cheng, Y.; Liu, X.; et al. Non-Hermitian topological whispering gallery. *Nature* **2021**, *597*, 655–659. [CrossRef]